We are IntechOpen, the world's leading publisher of Open Access books Built by scientists, for scientists

6,900
Open access books available

185,000
International authors and editors

200M
Downloads

154
Countries delivered to

Our authors are among the

TOP 1%
most cited scientists

12.2%
Contributors from top 500 universities

CLARIVATE ANALYTICS
BOOK CITATION INDEX
INDEXED

WEB OF SCIENCE™

Selection of our books indexed in the Book Citation Index
in Web of Science™ Core Collection (BKCI)

Interested in publishing with us?
Contact book.department@intechopen.com

Numbers displayed above are based on latest data collected.
For more information visit www.intechopen.com

DNS for Turbulent Premixed Combustion

Dipal Patel and Martin Agelin-Chaab

Abstract

Most of practical combustion occurs in turbulent flows which involve strong coupling between turbulence and chemical processes. The heat release from combustion alters the fluid properties such as density and viscosity and in turns affects the turbulence. Direct numerical simulations (DNS) provides a tool for obtaining both temporally and spatially resolved data in three dimension (3D). This chapter presents a brief overview of importance of DNS in turbulent combustion, the role of turbulence and identifies different combustion modes. The mathematical formulation and numerical implementation for DNS are introduced. The second half of this chapter presents DNS results for ignition in both homogeneous and stratified mixtures. It has been found that minimum ignition energy is required to obtain successful ignition in different turbulence regimes. An increase in turbulent velocity fluctuation may leads to a misfire. Additionally the difference between growing flames and those which are quenched by turbulence have been discussed with the help of the reaction–diffusion balance analysis. Furthermore, the turbulence intensity and length scale of the mixture inhomogeneity have important influences on achieving self-sustained combustion following successful ignition events.

Keywords: premixed combustion, turbulent premixed regimes, Kolmogorov scale, flame structure, ignition

1. Introduction

Many different numerical methods have been developed for the solution of fluid flow problems. Many commercial computational fluid dynamics (CFD) codes are available and have become standard engineering tools for simulation of non-reacting flows. However, for combustion, CFD techniques are not well developed for its accuracy and robustness. The moment we introduce combustion in CFD, it invites additional complexities for stable, accurate and efficient reacting flow numerical solvers. Many standard CFD techniques are available and serve as basic methods for solving combustion problems. Reader can refer to many standard textbooks on the subject [1, 2].

Direct numerical simulations (DNS) is a CFD tool which resolves all flow features explicitly and is widely adopted in combustion research. The feasibility and challenges of DNS in tackling the problems of turbulent combustion is discussed in great detail by Cant [3]. DNS often demands a very large computational power, especially when resolving the forced ignition process of turbulent reacting flows. Despite the computation cost, DNS is highly accurate and provides an enormous

amount of detailed information in comparison to experiments because it is either extremely expensive or impossible to obtain three-dimensional temporally and spatially resolved data by experimental means.

2. Why DNS?

There are three main strategies adopted in CFD simulations of turbulent flows. These strategies are:

- Reynolds averaged Navier–Stokes (RANS)

- Large eddy simulation (LES)

- Direct numerical simulation (DNS)

The philosophies of the above mentioned strategies can be understood from **Figure 1**, which illustrates the grid spacing requirements for DNS, RANS, and LES in relation to the turbulent kinetic energy spectrum $E(\kappa)$. In the RANS, the grid spacing (let us say Δx) is of the order of the inverse of energy containing wave number (i.e. $\Delta x \sim 1/l$), which tells us that the whole of the turbulent kinetic energy is unresolved in the context of RANS. In the LES, the grid size is close to the filter width Δ, which tells us that the physical processes are taking place for the wave number $\kappa < 1/\Delta$ are fully resolved, however, the physics at $\kappa > 1/\Delta$ are happening at subgrid level and thus remains unresolved. In the case of DNS, almost all the turbulent kinetic energy is resolved as the grid size is of the order of inverse of dissipation wave number. **Figure 2** shows the volume rendered of burnt products (blue), flame surface (red) and fresh reactants (transparent) in the computational cubic domain with comparison across three strategies. RANS only shows the statistical information of turbulence scales, whereas DNS provides time dependent instantaneous full information on turbulence scales with huge Reynolds number dependency.

In DNS turbulent fluid motion is simulated without any kind of physical approximation which indicates that you do not need any turbulence model for DNS,
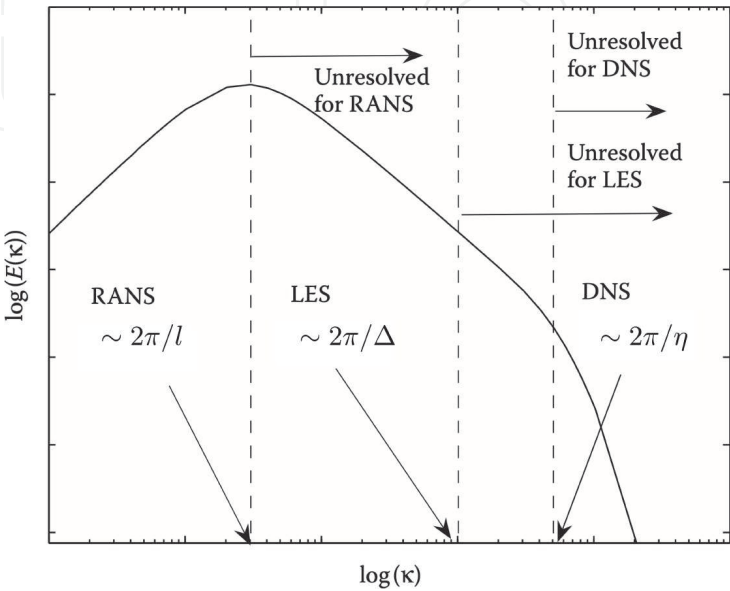

Figure 1.
The grid spacing for RANS, LES, and DNS on turbulent kinetic energy spectrum.
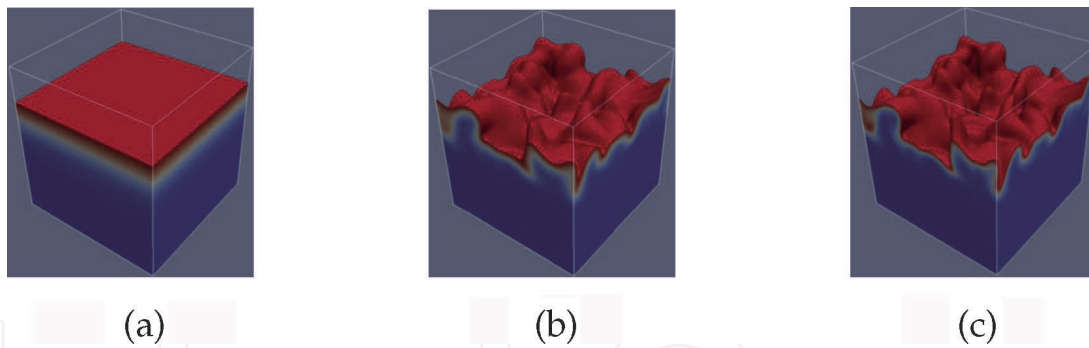
Figure 2.
Volume rendered view of reactants and products for (a) RANS, (b) LES, and (c) DNS.

all the length, time and velocity scales of turbulent flow are adequately resolved with the help of computational grid and time step used for given simulation case. It is important that the grid size (let us say Δx) in DNS needs to be smaller than the smallest significant length scale of turbulence, which is the Kolmogorov length scale η. Additionally, it is also important to have DNS computational domain that contains number of integral length scales so that enough number of large eddies are available to extract meaningful statistics. DNS simulations should be carried out for a number of integral time scales to have turbulent statistics that is independent of initial velocity field. The time step size for DNS should be smaller than the smallest time scale of turbulence. The computational time can be estimated by the product of grid points and number of time steps. This makes DNS extremely computationally expensive in nature. However, for case of compressible flow, computational time for DNS depends on Courant number, acoustic velocity, and Mach number.

3. Turbulent combustion

Combustion requires fuel and oxidiser to mix at the molecular level. How this takes place in turbulent combustion that depends on the turbulent mixing process. The general view is that once a range of different size eddies has developed, strain rate at the interface between the eddies enhances the mixing. During the eddy break-up process and the formation of smaller eddies, strain rate increases and thereby steepens the concentration gradients at the interface between reactants, which in turn enhances their molecular diffusion rate. Molecular mixing of fuel and oxidizer, a prerequisite of combustion, takes place at the interface between small eddies [4]. The subject of turbulent combustion spans a broad range of disciplines ranging from turbulent flows to combustion chemistry, which makes the analysis of turbulent combustion a daunting task. At the heart of the challenge is the presence of a broad range of length and time scales of the various processes governing combustion and the degree of coupling between these processes across all scales [5].

3.1 Turbulent scales

In order to estimate whether the chemistry is fast or slow compared to turbulent mixing, it is useful to define the time, length and velocity scales associated with physical processes. First consider the range of length scale (eddy sizes) that one may expect to encounter in turbulent flows. The largest length scale of turbulence is known as the integral length scale (L_{11}), which is the length scale at which most of the energetic eddies are associated. By contrast, the smallest length scale of turbulence known as Kolmogorov length scale, is determined by viscous dissipation of

turbulent kinetic energy. From the Kolmogorov's hypothesis, the only factors influencing the behavior of the small scale motions are the overall kinetic energy dissipation rate (ε) and the viscosity (ν). The length scale which governs these physical mechanisms is given by:

$$\eta = \left(\frac{\nu^3}{\varepsilon}\right)^{1/4} \tag{1}$$

This length scale is called the Kolmogorov length scale (η) and is the smallest hydrodynamic scale in turbulent flows. The kinetic energy of the flow is proportional to (u'^2), where u' is the velocity fluctuation. The time scale of the life time of the large eddies (commonly referred to as the large eddy turnover time) can be estimated as L_{11}/u'. Therefore, the kinetic energy dissipation rate is:

$$\varepsilon \sim \frac{u'u'}{L_{11}/u'} \sim \frac{(u')^3}{L_{11}} \tag{2}$$

The ratio of the largest to smallest length scales in the turbulent flow is given by:

$$\frac{L_{11}}{\eta} \sim \left(\frac{u'L_{11}}{\nu}\right)^{3/4} \sim Re_t^{3/4} \tag{3}$$

where Re_t is the turbulent Reynolds number. Another commonly encountered length scale in turbulence is the Taylor micro-scale. This length scale does not have the same easily understood physical significance as the Kolmogorov or internal length scale but provides a convenient estimate for the fluctuating strain rate field. The Taylor micro-scale (λ) is defined through the relation:

$$\varepsilon \sim \nu \frac{\partial u'_i}{\partial x_j}\frac{\partial u'_i}{\partial x_j} \sim \frac{u'^2}{\lambda^2} \tag{4}$$

The large eddy turnover time (t_e) can be defined as $t_e \sim L_{11}/u'$. The life time for the small eddies of turbulence can be estimated using the viscosity and the dissipation rate as $t_\eta \sim \sqrt{\nu/\varepsilon}$. The ratio of time scales is therefore:

$$\frac{t_e}{t_\eta} \sim \left(\frac{u'L_{11}}{\nu}\right)^{1/2} \sim Re_t^{1/2} \tag{5}$$

The large scale structures in the flow are seen to have a much larger time scale (duration) than the smallest energy dissipating eddies. As the turbulent Reynolds number of the flow increases, the magnitude of the separation between both time and length scales increases. One can define computational time for DNS scales with Re_t^3.

3.2 Premixed turbulent combustion regimes

Diagrams defining regimes of premixed turbulent combustion in terms of velocity and length scale ratio have been proposed in a number of previous analyses [6–8]. For scaling purposes it is useful to assume equal diffusivities for all reactive scalars, Schmidt number $Sc = \nu/D$ equal to unity, where D is the mass diffusivity. Based on this one can define flame thickness as $l_f = D/S_b$ and flame time as

$t_f = D/S_b{}^2$, where S_b is the laminar burning velocity at given equivalence ratio. One can estimate the turbulent Reynolds number as:

$$Re_t \sim \frac{u'L_{11}}{S_b l_f} \tag{6}$$

Furthermore, one can quantify the separation between chemical time scale to the Kolmogorov time scale using Karlovitz number (Ka) as:

$$Ka \sim \frac{t_f}{t_\eta} \sim \frac{l_f^2}{\eta^2} \tag{7}$$

Figure 3 shows the the regime diagram for premixed turbulent combustion using the definition of Kolmogorov length scale. Moreover, **Figure 3** shows the typical working conditions realised in IC engines, gas turbines and counter flow regime on the regime diagram. Here the ratios u'/S_b and L_{11}/l_f may be expressed in terms of the two non-dimensional numbers Re_t and Ka as:

$$\frac{u'}{S_b} = Re_t \left(\frac{L_{11}}{l_f}\right)^{-1} = Ka^{2/3}\left(\frac{L_{11}}{l_f}\right)^{1/3} \tag{8}$$

The lines $Re_t = 1$ and $Ka = 1$ represents boundaries between different regimes of premixed turbulent combustion in **Figure 3**. Other boundaries of interest are the line $u'/S_b = 1$ which separated the wrinkled flamelets from the corrugated flamelets, and the line denoted by $Ka = 100$, which separates the thin reaction zones from broken reaction zones. The line $Re_t = 1$ separates all turbulent flame regimes characterised by $Re_t > 1$ from the laminar flame regime ($Re_t < 1$), which is situated in the lower-left corner of the diagram. In the wrinkled flamelet regime, where $u' < S_b$, the turnover velocity u' of even the integral eddies is not large enough to compete with the advancement of the flame front with the laminar burning velocity S_b. Laminar flame propagation therefore dominates over flame front corrugations by turbulence [8].

The corrugated flamelet regime is characterised by the inequalities $Re_t > 1$ and $Ka < 1$. The inequality indicates that $l_f < \eta$ (see Eq. (7)), which means that the entire
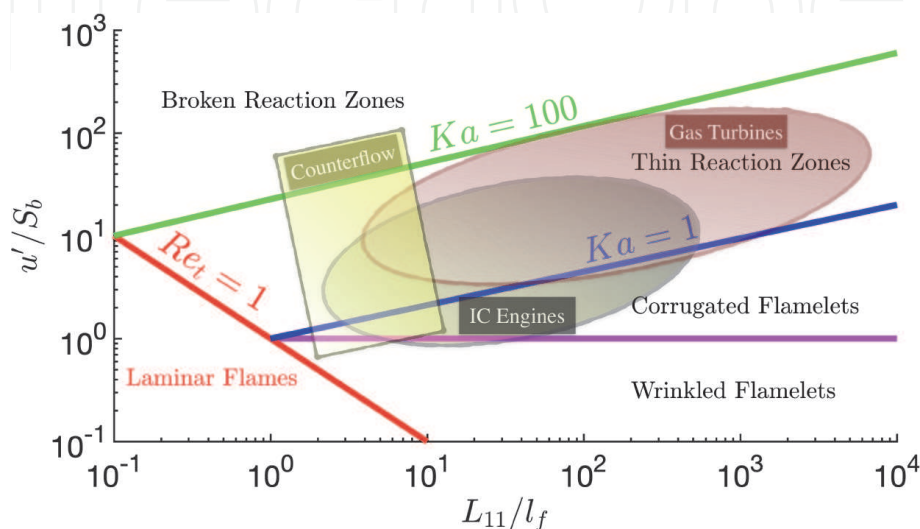

Figure 3.
Premixed turbulent combustion regime diagram accentuating areas for engineering applications.

Combustion regimes	Range
Laminar flames	$Re_t \leq 1$
Wrinkled flamelets	$Re_t \geq 1; u'/S_b \leq 1$
Corrugated flamelets	$Re_t \geq 1; u'/S_b > 1; Ka < 1$
Thin reaction zones[a]	$Re_t \geq 1; 1 \leq Ka < 100$
Broken reaction zones	$Re_t \geq 1; Ka \geq 100$

[a]*The analyses argued that since quenching by vortices occurs only for large Karlovitz numbers, the region below the limiting value of the Karlovitz number should corresponds to the flamelet regime [8].*

Table 1.
Summary of premixed turbulent combustion regimes.

reactive-diffusive flame structure is embedded within the eddies of the size of the Kolmogorov scale, where the flow is quasi-laminar. Therefore the flame structure is not perturbed by turbulent fluctuation and retains its quasi-laminar structure [8].

The thin reaction zones regime is characterised by $Re_t > 1$ and $1 < Ka < 100$, the last inequality indicating that the smallest eddies of size η can enter into the reactive–diffusive flame structure since $\eta < l_f$ (see Eq. (7)). These small eddies are still larger than the reaction layer thickness l_δ and can therefore not penetrate into that layer. The thickness δ of the inner layer in a premixed flame is typically one tenth of the flame thickness, such that l_δ is one tenth of the preheat zone thickness which is of the same order of magnitude as the flame thickness l_f.

Beyond the line $Ka = 100$ there is a regime called the broken reaction zones regime where Kolmogorov eddies are smaller than the inner layer thickness l_δ. These eddies may therefore enter into the inner layer and perturb it with the consequence that chemical processes are disturbed locally owing to enhanced heat loss to the preheat zone followed by temperature decrease and the loss of radicals. When this happens the flame will extinguish and fuel and oxidizer will inter diffuse and mix at lower temperatures where combustion reaction has ceased to take place. Nevertheless, regime diagram provides a useful purpose in allowing the classification of turbulent premixed flames, different premixed turbulent combustion regimes are summarised in **Table 1**.

4. Combustion modes: premixed and non-premixed

Generally, combustion can be divided into two categories: premixed and non-premixed combustion. **Figure 4** shows a Venn diagram representing different combustion modes. Each of these categories has their advantages and disadvantages, but premixed combustion offers advantages in terms of pollutant emission because the maximum burned gas temperature can be controlled by the mixture composition. Thus fuel lean premixed combustion can potentially lead to reduction of burned gas temperature which offers reduction in thermal NOx emission [9]. In the demand to reduce harmful emissions, industrial combustors are designed to operate under fuel lean conditions and with inhomogeneous mixtures, which increasingly often leads to stratified combustion [10, 11]. Many engineering combustion systems including: lean premixed prevaporised (LPP) gas turbine combustor, afterburners, and direct-injection spark-ignition internal combustion engines, they all operate in inhomogeneous reactants mode to gain full advantages of a spatially varying mixture field [12–14].
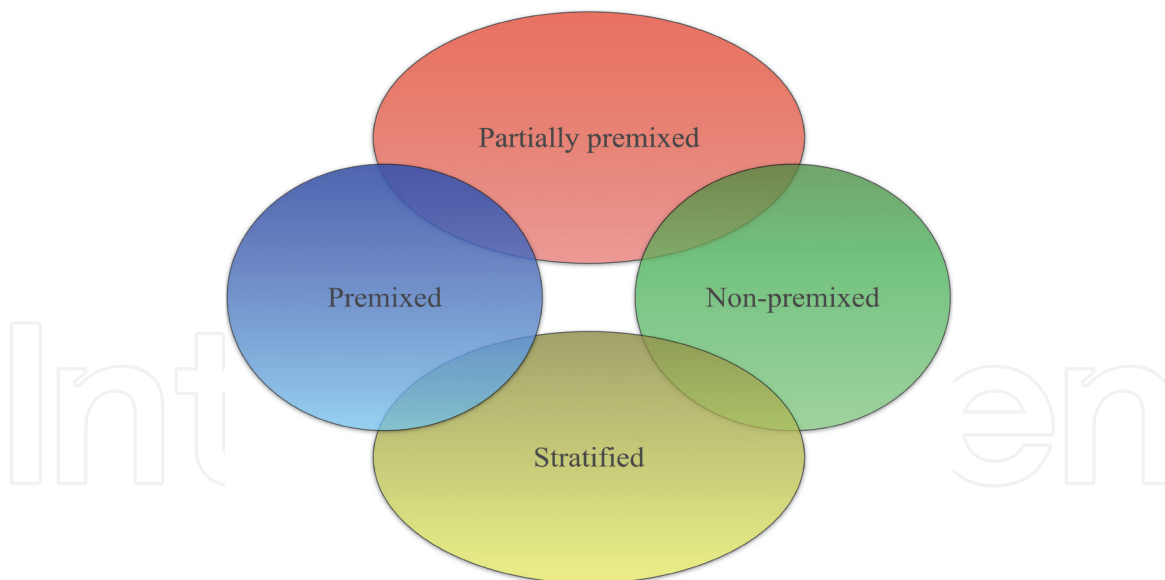
Figure 4.
Venn diagram representing combustion modes.

Stratified premixed combustion combines advantages of both premixed and non-premixed combustion modes (see **Figure 4**). In stratified combustion a premixed flame originated from ignition source travels through mixture field of varying equivalence ratio, which may be either all lean or all rich and the flame propagation is strongly affected by local gradient of mixture field [15]. For instant, in a gasoline direct injection (GDI) spark ignition engine, the time interval between fuel being injected into the combustion chamber and the spark ignition may be too short for the mixture composition to be homogeneous at the instant of ignition, but it is long enough for most of the fuel to be mixed with air before burning. The flame kernel originated by the spark propagates through a highly inhomogeneous mixture field characterised by large fluctuations in the equivalence ratio, with the ensemble-averaged mixture composition being lean (and even beyond lean flammability limit) in some spatial regions and rich (and even beyond the rich flammability limit) in other regions. In such example inhomogeneously premixed combustion is important, as it controls majority of the total heat release, while the afterburning of the lean and rich products in the diffusion mode may be of significant importance as far as pollutant (e.g. soot formation) is concerned. By contrast, in a diesel engine, the time interval between fuel injection and autoignition is too short that only a small amount of the fuel is mixed with air before autoignition of mixture due to compression. Here, also lean and rich premixed turbulent flames coexist with diffusion flames, but contrary to GDI engine, the total heat release is mainly controlled by the non-premixed mode of burning, and such regime is called nonpremixed/premixed combustion [7, 16]. All aforementioned combustion modes (stratified, premixed/nonpremixed, and nonpremixed/premixed burning) are commonly absorbed under partially-premixed flames [7].

5. DNS results and discussions

This section includes some of the DNS results of turbulent combustion in different environments. The results are presented and subsequently discussed. All the simulations presented here are performed using a well known compressible DNS code SENGA [3]. This DNS code solves the full compressible Navier-Stokes equations on a cartesian grid. The governing equations that describe the 3D gaseous

reacting flow consists of mass, momentum, energy and species conservation equations. The boundaries in the x_1–direction are taken to be partially non-reflecting and are specified using the Navier-Stokes characteristic boundary conditions (NSCBC) formulation [17], whereas the boundaries in the other directions are considered to be periodic. A 10th-order central difference scheme is used for spatial differentiation for the internal grid points, and the order of differentiation gradually reduces to a one-sided 2nd-order scheme at non-periodic boundaries [18]. The time advancement is carried out using a 3rd-order low-storage Runge–Kutta scheme [19].

5.1 Ignition

A source term q''' has been added for accounting the heat addition to the energy transport equation:

$$\frac{\partial \rho E}{\partial t} + \frac{\partial \rho u_k E}{\partial x_k} = -\frac{\partial u_k P}{\partial x_k} + \frac{\partial \tau_{ki} u_i}{\partial x_k} + \frac{\partial}{\partial x_k}\left[\lambda \frac{\partial \hat{T}}{\partial x_k}\right] + \dot{w}_T + q''' \qquad (9)$$

The specific heats at constant pressure and constant volume (i.e. c_p and c_v) are taken to be constant and same for all species for the simplified chemistry results. Therefore, the term $\sum_{k=1}^{N} h_{s,k} Y_k V_{k,i} = 0$ and not included in the Eq. (9). The source term is assumes to follow a Gaussian distribution [20] in the radial direction away from the centre of the igniter and can be expressed as:

$$q'''(r) = A_q \exp\left(-\frac{r^2}{2R^2}\right) \qquad (10)$$

where r is the radial distance from the centre of the igniter and R is the width of the Gaussian profile. The choice of R [21] in the present analysis allows sufficient resolution of the temperature gradient and guarantees the rapid disappearance of any artificial effects introduced by the ignition source. The constant A_q is determined by the following volumetric integration [21]:

$$\dot{Q} = \int_V q''' dV \qquad (11)$$

where $\dot{Q}$ is the ignition power, which can be defined as:

$$\dot{Q} = a_{sp} \rho_0 c_p \tau T_0 \left(\frac{4}{3}\pi l_f^3\right)\left[\frac{H(t) - H(t - t_{sp})}{t_{sp}}\right] \qquad (12)$$

where a_{sp} is a parameter that determined the total energy deposited by the igniter, the t_{sp} is the time duration over which the energy is deposited by the igniter, which is expressed as $t_{sp} = b_{sp} \times t_f$, where b_{sp} is the energy duration parameter and t_f is a characteristic chemical time scale given by $t_f = l_f/s_b$. The parameter b_{sp} varies between 0.2 and 0.4 for optimum spark duration according to experimental findings [22]. Here l_f is the Zel-dovich flame thickness for the stoichiometric mixture, which is defines as $l_f = \alpha T_0/S_b$, where αT_0 is the thermal diffusivity in the unburned reactants and S_b is the unstrained laminar burning velocity of the stoichiometric mixture. It is important to note that the details of the spark formation (momentum modification contribution, plasma formation and shock wave) remain

beyond the scope of the present analysis to keep this study computationally feasible. Parametric study of the effects of energy deposition characteristics (a_{sp} [parameter determining total energy deposition], b_{sp} [energy duration parameter] and R [parameter determining characteristic width of ignition energy deposition]) on localised forced ignition and early stages of burning following successful ignition in homogeneous turbulent mixtures using 3D DNS are investigated by [23, 24].

5.2 Ignition in homogeneous mixture

5.2.1 Isosurface of temperature field

Premixed combustion can be described in terms of a composition variable known as reaction progress variable. This reaction progress variable describe the progress of the premixed reaction [25]. The active scalars which are often considered for analysing turbulent combustion are the fuel mass fraction Y_F and the reaction progress variable c [26]. The extent of the completion of chemical reaction can be quantified in terms of a reaction progress variable c, defined as:

$$c = \frac{Y_{Fu} - Y_F}{Y_{Fu} - Y_{Fb}}$$ (13)

where Y_{Fu} is the fuel mass fractions in the unburned gas and Y_{Fb} is the fuel mass fraction in the burned gas. Both Y_{Fu} and Y_{Fb} are the function of mixture fraction. According to Eq. (13), c rises monotonically from zero in the fully unburned reactants to unity in the fully burnt products. **Figure 5** shows 3D volume rendered view of non-dimensional temperature for different Karlovitz numbers ranging across different turbulent regimes. The values for non-dimensional temperature T corresponds to reaction progress variable $c \geq 0.9$ showing the flame kernel. It is evident from **Figure 5** that the isosurfaces of T remains approximately spherical during the period of energy deposition, but they become increasingly wrinkled as time progresses for all the cases. During the energy deposition period (i.e. $t \leq t_{sp}$) the evolution of temperature field is principally determined by the diffusion of energy deposited, but after the ignition initiated, the flame propagation controlled by the diffusion of local flame stretching mechanism. The turbulence tends to fragment the flame surface and breaks the reaction zone for higher Karlovitz number cases. Furthermore interesting observation is when $t \gg t_{sp}$, the high temperature region has been fragmented thanks to energetic eddies of turbulence penetrating into the flame. This tendency is more prominent for $Ka = 150$, where turbulent eddies enters into flame and start breaking the reaction zone and flame eventually extinguishes.

5.2.2 Reaction-diffusion balance analysis

It is extremely important that heat release due to chemical reaction should overcome the heat transfer from the hot gas kernel in order to obtain self-sustained combustion following successful ignition. The transport equation of the reaction progress variable c in the context of turbulent premixed flames is:

$$\frac{\partial \rho c}{\partial t} + \frac{\partial \rho u_j c}{\partial x_j} = \frac{\partial}{\partial x_j}\left[\frac{\partial \rho D c}{\partial x_j}\right] + \dot{w}_c$$ (14)

where $\dot{w}_c$ is the reaction progress variable reaction rate.

(a) $Ka = 6.30$ at $2.1t_{sp}$, $6.4t_{sp}$ and $12.6t_{sp}$

(b) $Ka = 44.20$ at $2.1t_{sp}$, $6.4t_{sp}$ and $12.6t_{sp}$

(c) $Ka = 150$ at $2.1t_{sp}$, $6.4t_{sp}$ and $12.6t_{sp}$
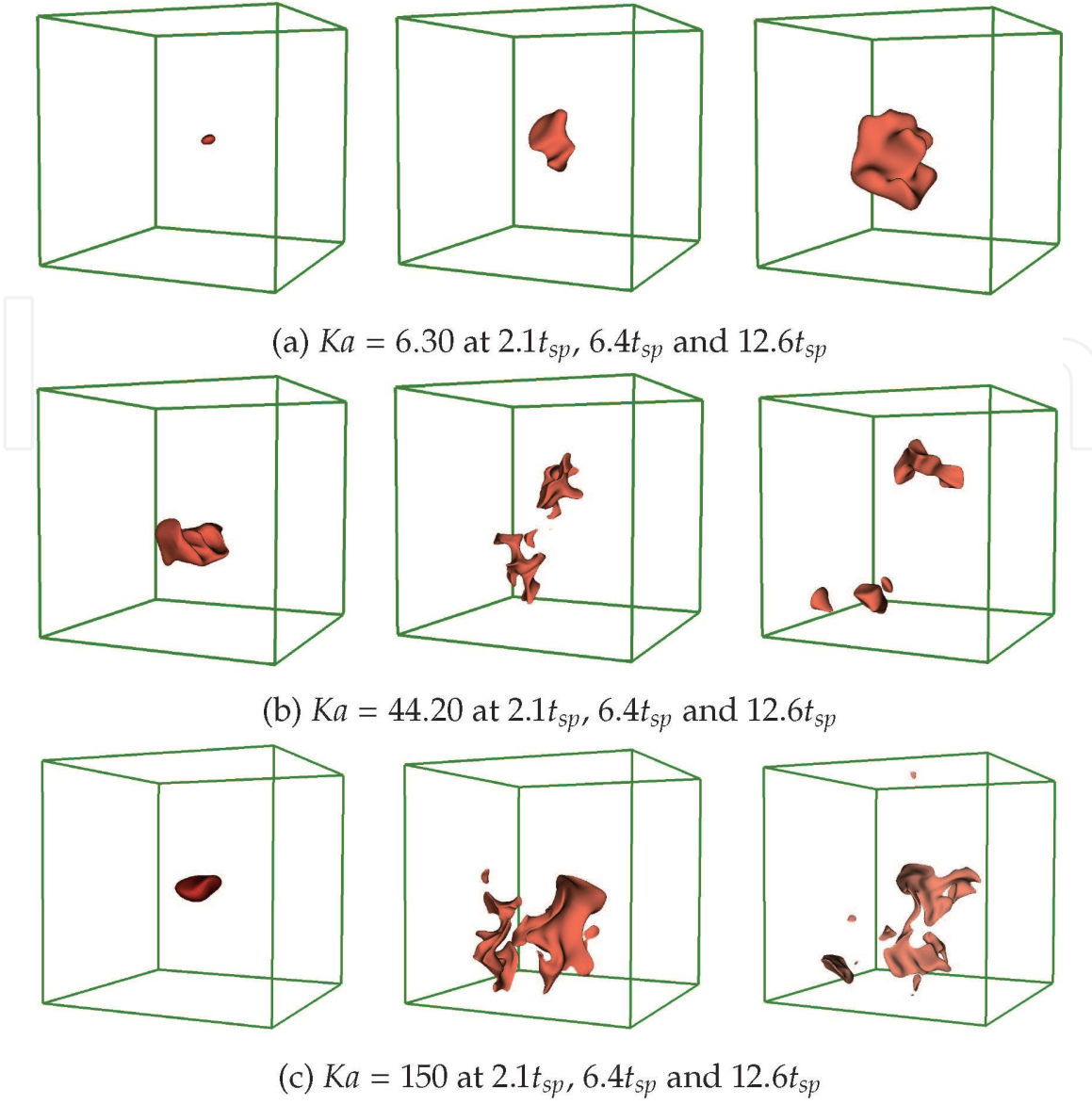
Figure 5.
Volume rendered view of non-dimensional temperature field in domain $51l_f \times 51l_f \times 51l_f$ for different Karlovitz numbers (Ka) in different turbulent regimes.

It is important to examine the reaction–diffusion balance in order to understand the difference in flame kernels which are growing in an unperturbed manner and those which are fragmented and about to be quenched by turbulence. In that respect, following terms are defined to explain the reaction–diffusion balance within the flame:

$$\text{reaction term}: \quad \dot{w}_c \tag{15}$$

$$\text{molecular diffusion term}: \quad \nabla \cdot (\rho D \nabla c) \tag{16}$$

$$\text{flame normal diffusion rate term}: \quad \vec{N} \cdot \nabla\left(\rho D \vec{N} \cdot \nabla c\right) \tag{17}$$

$$\text{tangential diffusion rate term}: \quad -\rho D \nabla \cdot \vec{N} |\nabla c| \tag{18}$$

where $\vec{N}$ is the flame normal vector, which can be defined as:
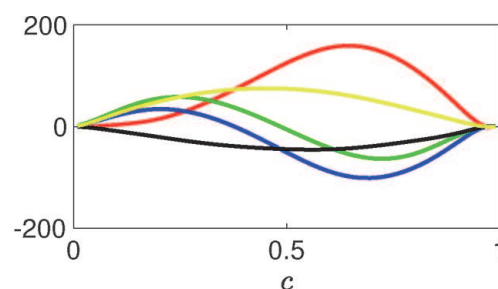
$$\vec{N} = -\frac{\nabla c}{|\nabla c|} \tag{19}$$

It can be seen from **Figure 6** that the term $\dot{w}_c$ (■) remains negligible in the unburned side and increases sharply towards the burned side before decreasing to zero in the fully burned products. The magnitude of this term decreases with time, once the igniter is switched off, which is principally due to the decrease in fuel reaction rate magnitude with time. Therefore, it can be seen that maximum reaction takes place in the region $0.6 \leq c \leq 0.99$. The term $\nabla \cdot (\rho D \nabla c)$ (■) shows opposite behaviour to the term $\dot{w}_c$ (■), suggesting reactants are diffusing prior to approaching the flame kernel and term remains negative in burned side. Additionally, the term $\dot{w}_c + \nabla \cdot (\rho D \nabla c)$ (■) suggests a self-sustained propagation of flame kernel. The term $\vec{N} \cdot \nabla \left(\rho D \vec{N} \cdot \nabla c \right)$ (■) remains positive in unburned side but becomes negative towards burned side. The term $-\rho D \nabla \cdot \vec{N} |\nabla c|$ (■) remains negative for the flame brush. In the flame normal vector, N_j is the jth component of flame normal which can be defined in terms of flame curvature [27]:

$$\kappa_m = \frac{1}{2} \nabla \cdot \vec{N} = \frac{\kappa_1 + \kappa_2}{2} \sim \frac{1}{R_{fk}} \tag{20}$$

where κ_1 and κ_2 are the two principle curvature of the concerned flame surface, κ_m is the arithmetic mean of these two principle curvatures and R_{fk} is the radius of a flame kernel. As the flame kernel increases in size (i.e. R_{fk} increases), the probability of high values of κ_m decreases (see Eq. (20)). Furthermore according to Eq. (20) positively curved location (i.e. $\kappa_m > 0$) are convex towards the reactant. The flame is initiated as a spherical kernel from the localised forced ignition, which has a positive mean curvature. In this respect the term $-\rho D \nabla \cdot \vec{N} |\nabla c|$ (■) will attain negative values in the case of expanding flame kernel (i.e. self-sustained propagating flame kernel). The growth of the kernel leads to a decrease in the magnitude of the negative contribution of the term $-\rho D \nabla \cdot \vec{N} |\nabla c|$ (■), whereas the term $-\rho D \nabla \cdot \vec{N} |\nabla c|$ (■) is expected to assume large negative values in the kernels which are quenching. This findings are in good agreement with previous experimental studies [28, 29].

5.3 Ignition in stratified mixture

Premixed combustion offers an option of controlling flame temperature and reducing pollutant emission such as nitrogen oxides (NOx) but, in practice, perfect mixing is often difficult to achieve and thus combustion in many engineering applications takes place in turbulent stratified mixtures. Many previous findings

$\dot{w}_c$ (■); $\nabla \cdot (\rho D \nabla c)$ (■); $\vec{N} \cdot \nabla (\rho D \vec{N} \cdot \nabla c)$ (■); $-\rho D \nabla \cdot \vec{N} |\nabla c|$ (■); $\dot{w}_c + \nabla \cdot (\rho D \nabla c)$ (■);

Figure 6.
Mean variation of different terms with reaction progress variable at $t = 2.6 t_{sp}$ for $Ka = 6.30$.
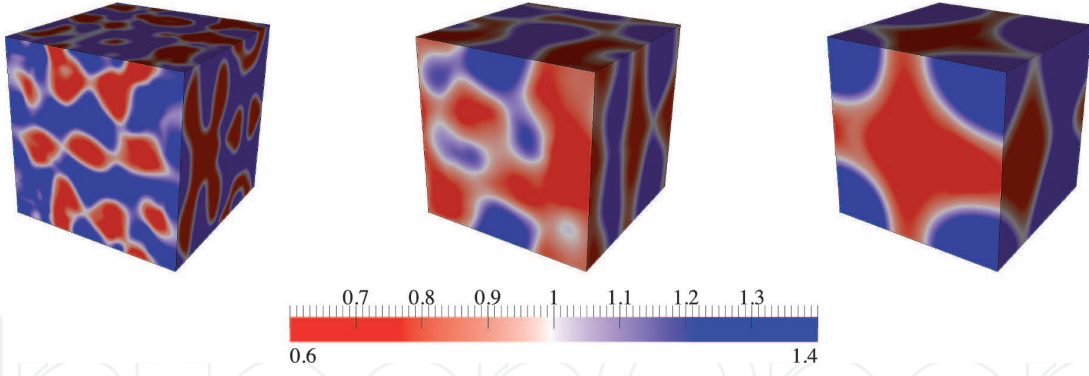
Figure 7.
Initial computational domain showing different values of length scale of mixture inhomogeneities, l_ϕ/l_f = 2.1 (left), =5.5 (middle), and =8.3 (right).

[30, 31] shows that the flame propagation statistics are strongly influenced by the local equivalence ratio gradient. The length scale of mixture inhomogeneity is taken as the Taylor micro-scale of the equivalence ratio variation l_ϕ and is defined as [32]:

$$l_\phi = \sqrt{\frac{6\langle [\phi - \langle\phi\rangle]^2 \rangle}{\langle \nabla[\phi - \langle\phi\rangle] \cdot \nabla[\phi - \langle\phi\rangle]\rangle}} \qquad (21)$$

The equivalence ratio ϕ variation is initialised using a random distribution of ϕ following a Bi-modal distribution for specified values of the mean global equivalence ratio $\langle\phi\rangle$. In practical, when fuel is introduced in the liquid phase, the probability density function (PDF) of the equivalence ratio distribution is likely to be Bimodal as a result of localised liquid fuel evaporation during the early stage of mixing. The fuel-air mixture is likely to be fuel rich close to the evaporation sites and the mixture is expected to be fuel-lean far away from the droplets. The initial mixture distribution for $\langle\phi\rangle = 1$ and $\phi' = 0.4$ with different values of l_ϕ/l_f are shown in **Figure 7**, which indicated that the clouds of mixture inhomogeneities increase in size with increasing l_ϕ/l_f.

5.3.1 Mode of combustion

The role of the reaction progress variable c, in the turbulent stratified mixtures has been discussed in detail by Bray et al. [33]. In the context of stratified combustion, the reaction progress variable can be defines in the following manner [21, 25]:

$$c = \frac{\xi Y_{F\infty} - Y_F}{\xi Y_{F\infty} - \max\left[0, \frac{\xi - \xi_{st}}{1 - \xi_{st}}\right] Y_{F\infty}} \qquad (22)$$

where ξ is the conserved scalar and can be defined as:

$$\xi = \frac{Y_F - \frac{Y_O}{s} + \frac{Y_{O\infty}}{s}}{Y_{F\infty} + \frac{Y_{O\infty}}{s}} \qquad (23)$$

where s is the mass of the oxidiser consumed per unit mass of fuel consumption, Y_F and Y_O are local fuel and oxidiser mass fractions respectively, $Y_{F\infty}$ is the fuel mass fraction in pure fuel stream and $Y_{O\infty}$ is the oxidiser mass fraction in air.

In order to understand the flame structure originating from localised forced ignition (e.g. spark or laser), the Takeno flame index [34, 35] can be used to identify the local combustion mode:

$$I_c = \frac{\nabla Y_F}{|\nabla Y_F|} \cdot \frac{\nabla Y_O}{|\nabla Y_O|} \qquad (24)$$

Based on Eq. (24), the Takeno flame index obtains positive value in premixed mode of combustion and negative value in non-premixed mode of combustion. The volume rebdered views of the region corresponding to $0.01 \leq c \leq 0.99$ coloured with local values of I_c at $t = 8.40t_{sp}$ are shown in **Figure 8** for selected cases. It is evident from **Figure 8** that the reaction takes place predominantly in the premixed mode (i.e. $I_c > 0$) but some pockets of $I_c < 0$ indicate the possibility of finding local pockets of non-premixed combustion. The probability of finding $I_c < 0$ decreases with increasing time due to mixing process. The I_c predominantly assumes positive values and major portion of overall heat release arises due to the premixed mode of combustion in all cases. Moreover, the percentage of heat release arising from the non-premixed mode of combustion decreases with increasing value of u' as a result of improved mixing.
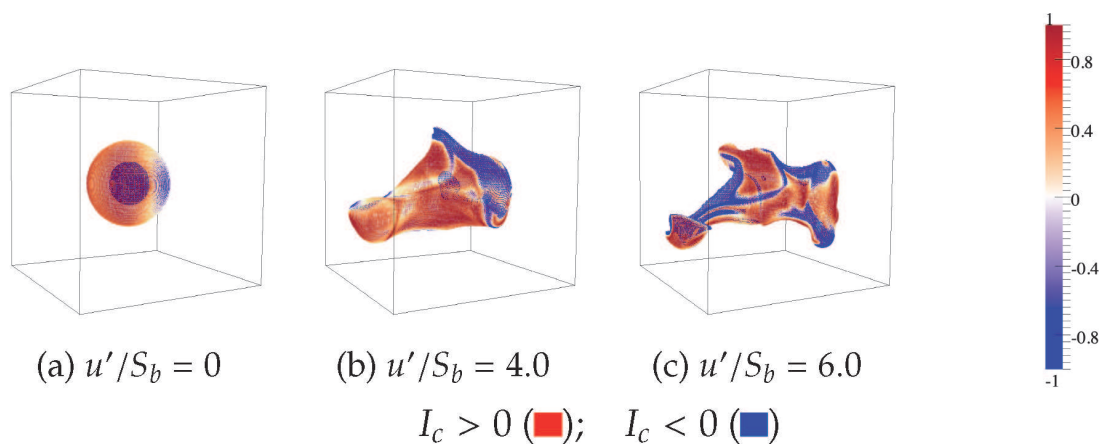

(a) $u'/S_b = 0$ (b) $u'/S_b = 4.0$ (c) $u'/S_b = 6.0$

$$I_c > 0 \;(\blacksquare); \quad I_c < 0 \;(\blacksquare)$$

Figure 8.
Volumetric rendering of the region corresponding to $0.01 \leq c \leq 0.99$ in domain $33l_f \times 33l_f \times 33l_f$ coloured with local values of I_c for different values of u'/S_b and mixture inhomogeneity $l_\phi/l_f = 8.3$.

(a) $u'/S_b = 0$ (b) $u'/S_b = 4.0$

$$l_\phi/l_f = 2.1 \;(\blacksquare); \quad l_\phi/l_f = 5.5 \;(\blacksquare); \quad l_\phi/l_f = 8.3 \;(\blacksquare)$$
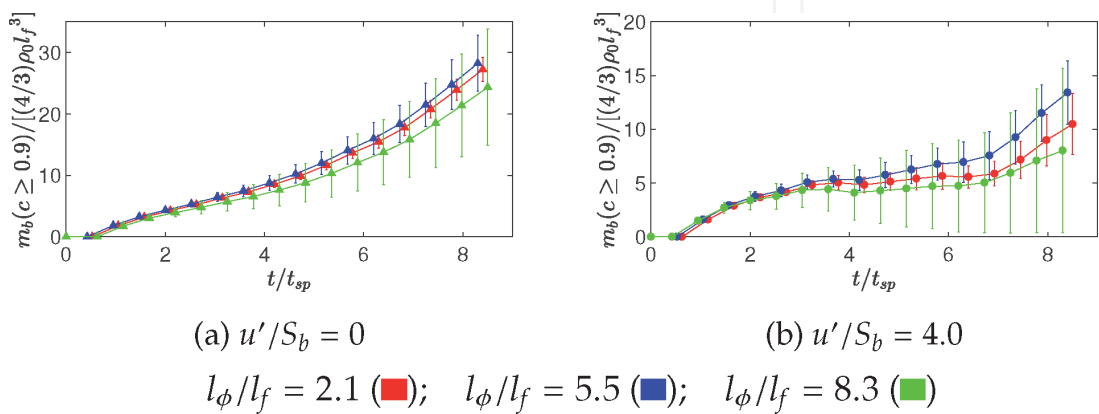
Figure 9.
Temporal evolution of mean burnt gas mass with $\phi' = 0.2$ and $l_\phi/l_f = 5.5$ with standard deviation due to different realisation of initial conditions shown in the form of bars.

5.3.2 Extent of burning

The extent of burning can be characterised by the mass of burned gas m_b with $c \geq 0.9$ [21]. The temporal evolution of burnt gas mass normalised by the mass of an unburned gas sphere with a radius equal to l_f for $l_\phi/l_f = 5.5$ are show in **Figure 9**. It is important to note that $\int_V \rho c \, dV$ provides the measure of total burned gas mass within the computational domain. **Figure 9** shows that an increase in u' leads to reduction in burned gas mass for all cases. An increase in u' leads to an increase in eddy diffusivity $D_t \sim u'L_{11}$ for a given high values of turbulence intensity. For self-sustained flame propagation following successful ignition, the heat release from the combustion must overcome the heat loss from hot gas kernel. Due to heat transfer from hot gas kernel, the probability of $c \geq 0.8$ also decreases and at such point the heat loss overcomes chemical heat release, the hot gas kernel shrinks and eventually leads to flame extinction. The detrimental effect of u' on the extent of burning is consistent with previous findings [36]. The influence of l_ϕ/l_f on the extent of burning is found to be non-monotonic and dependent on ϕ'. For high values of l_ϕ/l_f the clouds of mixture stratification are relatively big and as a result of this, there is a possibility that igniter has encountered a rich region (highly flammable) of mixture which leads to higher burning rate. It is well known that combustion succeeds only for selected realisation of initial distribution of ϕ and this aspect is particular interest in the cylinder of IC engines due to cycle-to-cyle variation [20]. The temporal evolution of mean and standard deviations of burnt gas mass for all realisations are shown in **Figure 9** to demonstrate the probabilistic nature of the localised ignition of stratified mixtures. Furthermore, the large variation of error bar for hight values of l_ϕ/l_f suggests that it is possible to obtain large clouds of both highly flammable and weakly flammable mixtures at the igniter location which leads to large variation of burnt gas mass.

The above discussion suggests that turbulent intensity u' and length scale of mixture inhomogeneity l_ϕ have important influences on achieving self-sustained combustion following successful ignition event.

6. Epilogue

Theories and results presented in this chapter suggests that turbulent premixed combustion is a complex and difficult subject, but very rich in the physics. With recent advances in computational capability, the application of DNS will become possible for higher values of turbulent Reynolds number and complex flow configurations. DNS provides highly accurate and detailed 3D information in comparison to experiments because it is extremely expensive or impossible to obtain 3D temporally and spatially resolved data by experimental means. However, with current advances in laser technology, it is possible to have simultaneous planer laser-induced measurement of turbulent concentration and velocity fields. Once this experimental data becomes available, it will be used for validation of DNS results. Moreover, successful ignition often leads to momentum modification contribution, plasma formation, and shock waves, which remains beyond the scope of the present DNS analysis. Additionally, detailed chemical mechanism involving large number of intermediate species which lead to back-diffusion of light radical and post diffusion flames are necessary to gain further fundamental understanding of turbulent combustion processes.

Acknowledgements

Authors are grateful to facilities of Compute Canada for computational support. The author gratefully acknowledge the training he receive from his supervisor Prof. N. Chakraborty. The author also acknowledge the practical help and valuable discussion with Dr. Jiawei Lai, Dr. Sahin Yigit and Dr. Bruno Machado while preparing the manuscript.

Conflict of interest

The authors declare no conflict of interest.

Author details

Dipal Patel[†] and Martin Agelin-Chaab*[†]
Department of Automotive, Mechanical and Manufacturing Engineering, Faculty of Engineering and Applied Science, Ontario Tech University, Oshawa, ON, Canada

*Address all correspondence to: martin.agelin-chaab@uoit.ca

† These authors contributed equally.

IntechOpen

References

[1] Hirsch C. Numerical and Computation of Internal and External Flows: The Fundamentals of Computational Fluid Dynamics. Elsevier; 2007

[2] Roache PJ. Fundamentals of Computational Fluid Dynamics. Albuquerque, NM: Hermosa Publishers; 1998

[3] Cant S. Direct numerical simulation of premixed turbulent flames. Philosophical Transactions of the Royal Society of London. Series A: Mathematical, Physical and Engineering Sciences. 1999;**357**(1764):3583-3604

[4] Poinsot T, Veynante D. Theoretical and Numerical Combustion. RT Edwards, Inc.; 2005. ISBN 1930217102

[5] Echekki T, Mastorakos E. Turbulent Combustion Modeling: Advances, New Trends and Perspectives, Volume 95. Springer Science & Business Media; 2010. ISBN: 9400704127

[6] Bradley D, Lung FK-K. Spark ignition and the early stages of turbulent flame propagation. Combustion and Flame. 1987;**69**(1):71-93

[7] Lipatnikov A. Fundamentals of Premixed Turbulent Combustion. CRC Press; 2012. ISBN: 1466510250

[8] Peters N. Turbulent Combustion. Cambridge University Press; 2000

[9] McAllister S, Chen J-Y, Carlos Fernandez-Pello A. Fundamentals of Combustion Processes. Vol. 302. New York: Springer; 2011

[10] Alkidas AC. Combustion advancements in gasoline engines. Energy Conversion and Management. 2007;**48**(11):2751-2761

[11] Drake MC, Haworth DC. Advanced gasoline engine development using optical diagnostics and numerical modeling. Proceedings of the Combustion Institute. 2007;**31**(1):99-124

[12] Brosh T, Patel D, Wacks D, Chakraborty N. Numerical investigation of localized forced ignition of pulverized coal particle-laden mixtures: A Direct Numerical Simulation (DNS) analysis. Fuel. 2015;**145**:50-62

[13] Lim KM. DNS of inhomogeneous reactants premixed combustion [PhD thesis]. Fitzwilliam College; 2015

[14] Mongia HC, Held TJ, Hsiao GC, Pandalai RP. Challenges and progress in controlling dynamics in gas turbine combustors. Journal of Propulsion and Power. 2003;**19**(5):822-829

[15] Swaminathan N, Grout R, Mastorakos E. Direct simulations of forced ignition in stratified mixture. In: Proceedings of the Third European Combustion Meeting. 2007

[16] Bilger RW, Pope SB, Bray KNC, Driscoll JF. Paradigms in turbulent combustion research. Proceedings of the Combustion Institute. 2005;**30**(1):21-42

[17] Poinsot TJ, Lelef SK. Boundary conditions for direct simulations of compressible viscous flows. Journal of Computational Physics. 1992;**101**(1): 104-129

[18] Jenkins KW, Cant RS. Flame kernel interactions in a turbulent environment. In: Technical Report. Cambridge University; 2001

[19] Wray AA. Minimal storage time advancement schemes for spectral methods. In: Report No. MS 202. California: NASA Ames Research Center; 1990

[20] Pera C, Chevillard S, Reveillon J. Effects of residual burnt gas

heterogeneity on early flame propagation and on cyclic variability in spark-ignited engines. Combustion and Flame. 2013;**160**(6):1020-1032

[21] Patel D, Chakraborty N. Localised forced ignition of globally stoichiometric stratified mixtures: A numerical investigation. Combustion Theory and Modelling. 2014;**18**(6):627-651

[22] Ballal D, Lefebvre A. Spark ignition of turbulent flowing gases. Aerospace Research Central. 1977:185

[23] Patel D, Chakraborty N. Effects of energy deposition characteristics on localised forced ignition of homogeneous mixtures. International Journal of Spray and Combustion Dynamics. 2015;**7**(2):151-174

[24] Patel D, Chakraborty N. Effects of fuel Lewis number on localised forced ignition of turbulent homogeneous mixtures: A numerical investigation. International Journal of Spray and Combustion Dynamics. 2016;**8**(3):183-196

[25] J Hélie and A Trouvé. Turbulent flame propagation in partially premixed combustion. In Turbulent Flame Propagation in Partially Premixed Combustion, volume 27, pages 891–898. Elsevier, 1998. ISBN 0082-0784

[26] Malkeson SP, Chakraborty N. Statistical analysis of displacement speed in turbulent stratified flames: A direct numerical simulation study. Combustion Science and Technology. 2010;**182**(11–12):1841-1883

[27] Chakraborty N, Mastorakos E. Numerical investigation of edge flame propagation characteristics in turbulent mixing layers. Physics of Fluids. 2006;**18**(10):105103

[28] Ahmed SF, Mastorakos E. Spark ignition of lifted turbulent jet flames. Combustion and Flame. 2006;**146**(1–2): 215-231

[29] Chung SH. Stabilization, propagation and instability of tribrachial triple flames. Proceedings of the Combustion Institute. 2007;**31**(1): 877-892

[30] Haworth DC, Blint RJ, Cuenot B, Poinsot TJ. Numerical simulation of turbulent propane–air combustion with nonhomogeneous reactants. Combustion and Flame. 2000;**121**(3): 395-417

[31] Anselmo-Filho P, Hochgreb S, Barlow RS, Cant RS. Experimental measurements of geometric properties of turbulent stratified flames. Proceedings of the Combustion Institute. 2009;**32**(2):1763-1770

[32] Eswaran V, Pope SB. Direct numerical simulations of the turbulent mixing of a passive scalar. The Physics of fluids. 1988;**31**(3):506-520

[33] Bray K, Domingo P, Vervisch L. Role of the progress variable in models for partially premixed turbulent combustion. Combustion and Flame. 2005;**141**(4):431-437

[34] Hannebique G, Sierra P, Riber E, Cuenot B. Large eddy simulation of reactive two-phase flow in an aeronautical multipoint burner. Flow, Turbulence and Combustion. 2013; **90**(2):449-469

[35] Lignell D, Chen JH, Lu T, Law CK. Direct numerical simulation of extinction and reignition in a nonpremixed turbulent ethylene jet flame. In: Technical Report. Sandia National Lab.; 2007

[36] Richardson ES, Mastorakos E. Numerical investigation of forced ignition in laminar counterflow non-premixed methane-air flames. Combustion Science and Technology. 2007;**179**(1–2):21-37